

# FLUX-CONSERVING FINITE ELEMENT METHODS

SHANGYOU ZHANG, ZHIMIN ZHANG, AND QINGSONG ZOU

**ABSTRACT.** We analyze the flux conservation property of the finite element method. It is shown that the finite element solution does approximate the flux locally in the optimal order, i.e., the same order as that of the nodal interpolation operator. We propose two methods, post-processing the finite element solutions locally. The new solutions, remaining as optimal-order solutions, are flux-conserving elementwise. In one of our methods, the processed solution also satisfies the original finite element equations. While the high-order finite volume schemes are still under construction, our methods produce finite-volume-like finite element solution of any order. In particular, our methods avoid solving non-symmetric finite volume equations. Numerical tests in 2D and 3D verify our findings.

**AMS subject classifications.** Primary 65N30; Secondary 45N08

**Key words.** High order, finite volume method, flux conservation, finite element method

## 1. INTRODUCTION

The finite element method (FEM) is a most popular method in solving partial differential equations, cf. [3]. Due to its local conservation property of flux, the finite volume method (FVM) is also used in a wide range of computation, especially in computational fluid dynamics, cf. [15, 19]. However, the mathematical theory on FVM (cf., [12, 15, 16]) has not been fully developed, at least, not as satisfactory as that for FEM. Low order FVM theory ( $P_1$  and some  $P_2$  methods) is well established, see e.g., [2, 5, 7, 11, 13, 16]. Both the design and analysis on high order, symmetric FVMs are still under investigation, see [6, 8, 9, 18, 20, 22, 24].

In this paper, we seek flux-conserving solutions in a completely different way. The basic idea is to do a post processing on the finite element solution so that the new solution is flux conserving elementwise. To this end, we first analyze the flux-conservation property of the finite element solution. It is shown that the order of approximation of finite element in flux is optimal, the same order as that of nodal interpolation. The order is  $O(h^{k-1})$  for the  $k$ -th degree finite element. That is, there is no convergence in total flux when using linear ( $P_1$ ) finite element. This is

---

This author is partially supported by the US National Science Foundation through grant DMS-0612908, the Ministry of Education of China through the Changjiang Scholars program, and Guangdong Provincial Government of China through the “Computational Science Innovative Research Team” program.

also confirmed numerically, both in 2D and 3D. To overcome this shortcoming of finite element method, we correct the flux error locally on each element by bubble functions, cf. Figure 1. In one method, we use the same order bubbles, cubic bubbles in 2D and quartic bubbles in 3D, for any order finite element method. In the second method, we use degree- $(k + 2)$  orthogonal bubbles for the  $k$ -th degree finite element solutions. In the latter method, the post-processed finite element solution still satisfies the original finite element equations. In both methods, the post-processed finite element solution remains as an optimal-order solution, in both  $H^1$  and  $L^2$  norms.

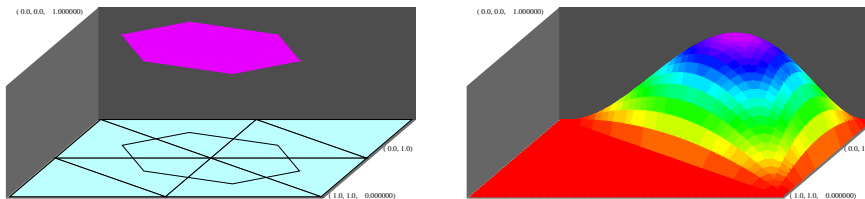


FIGURE 1. A finite volume test function, and a cubic bubble function.

We note that the finite volume solution is flux-conserving on each dual cell, i.e., control-volume, see the left graph in Figure 1. However for most high-order FVM solutions, the approximate theory has not been established cf. [8, 9, 23, 24]. Also, other than  $P_1$  FVM for constant coefficient problems, it is not natural to derive symmetric FVM, cf. [14, 17] and references therein. This is important for eigenvalue problems [10], even in dealing low order terms. On the other hand, symmetric, high-order finite element equations are naturally defined, by the orthogonal projection in a Hilbert space, [3]. Such high-order finite element equations can be solved effectively by the multigrid method or other fast solvers [3, 21]. At the end, we correct the finite element solutions by bubble functions, to obtain flux-conserving solutions. Such a correction does not alter the value of the finite element solution on the inter-element boundary, i.e., on vertices, edges, and triangles (in 3D).

The rest of manuscript is organized as follows. In Section 2, we introduce the finite element method and analyze its flux approximation. In Section 3, we define a post-processing algorithm. We will show the flux-conserving property of the processed solution and its optimal order of convergence. In Section 4, we provide numerical examples in 2D and 3D. Some remarks are made in Section 5.

## 2. ON FLUX-CONSERVATION PROPERTY OF STANDARD FEM

Let  $\Omega$  be a bounded, polygonal domain in  $\mathbb{R}^d$ ,  $d \geq 2$ . We consider the following second-order elliptic boundary value problem

$$(2.1) \quad -\nabla \cdot (\alpha(\mathbf{x})\nabla u) = f \quad \text{in } \Omega,$$

$$(2.2) \quad u = 0 \quad \text{on } \Gamma,$$

where the boundary  $\Gamma = \partial\Omega$  and  $\alpha(\mathbf{x})$  is a bounded and piecewise continuous function that is bounded below: There exists a constant  $\alpha_0 > 0$  such that  $\alpha(\mathbf{x}) \geq \alpha_0$  for almost all  $x \in \Omega$ . We choose homogeneous Dirichlet boundary condition here only for simplicity of presentation. The analysis is similar for other boundary conditions.

Let  $\mathcal{T}_h$  be a quasi-uniform, and shape-regular simplicial *triangulation* on the domain  $\Omega$  :

$$\mathcal{T}_h = \{\tau \mid \text{diam}(\tau) \leq h < 1\}.$$

With respect to  $\mathcal{T}_h$ , we define an order  $k$  finite element subspace

$$(2.3) \quad U_h := \{v \in C(\overline{\Omega}) : v|_{\tau} \in \mathcal{P}_k, \text{ for all } \tau \in \mathcal{T}_h, v|_{\partial\Omega} = 0\},$$

where  $\mathcal{P}_k$  is the space of all polynomials of degree equal to or less than  $k$ . Thus,  $U_h \subset H_0^1(\Omega)$ . The finite element solution of (2.1) and (2.2) is a function  $u_h \in U_h$  such that

$$(2.4) \quad a(u_h, v_h) = (f, v_h) \quad v_h \in U_h,$$

where the bilinear form  $a(\cdot, \cdot)$  is defined by

$$a(v, w) = \int_{\Omega} \alpha(\mathbf{x})\nabla v \cdot \nabla w \, d\mathbf{x} \quad \forall v, w \in H_0^1(\Omega),$$

and the inner product  $(\cdot, \cdot)$  is defined by

$$(v, w) = \int_{\Omega} vw \, d\mathbf{x} \quad \forall v, w \in L^2(\Omega).$$

Unlike the finite volume solutions, the FEM solution  $u_h$  in (2.4) does not satisfy the following conservation law elementwise

$$\int_{\tau} f \, d\mathbf{x} + \int_{\partial\tau} \alpha(\mathbf{x}) \frac{\partial u_h}{\partial \mathbf{n}} \, ds \neq 0 \quad \forall \tau \in \mathcal{T}_h.$$

We will define a post-processing method next section so that the above flux-error is zero elementwise. But we will show first that the finite element solution does preserve flux locally in certain degree. In this paper, we adopt a notation  $\lesssim$ , for “ $\leq C$ ”, where  $C$  is a generic, positive constant, independent of the grid size  $h$ , and some other parameters. That is, “ $A \lesssim B$ ” means that  $A$  can be bounded by  $B$  multiplied by a constant which is independent of the parameters which  $A$  and  $B$  may depend on.

**Theorem 2.1.** *Let  $u \in H^{k+1}(\Omega)$  solve (2.1)–(2.2) and  $u_h$  solve (2.4). It holds that*

$$(2.5) \quad \sum_{\tau \in \mathcal{T}_h} \left| \int_{\tau} f \, d\mathbf{x} + \int_{\partial\tau} \alpha(\mathbf{x}) \frac{\partial u_h}{\partial \mathbf{n}} \, ds \right| \lesssim h^{k-1} |u|_{H^{k+1}},$$

where the hidden constant depends only on  $\alpha(\mathbf{x})$  and the shape-regularity of  $\mathcal{T}_h$ .

*Proof.* For all  $\tau \in \mathcal{T}_h$ , by (2.1) and the divergence theorem,

$$\int_{\tau} f \, d\mathbf{x} = - \int_{\partial\tau} \alpha(\mathbf{x}) \frac{\partial u}{\partial \mathbf{n}} \, ds.$$

By (2.4), the finite element solution has a local flux-error,

$$(2.6) \quad \int_{\tau} f \, d\mathbf{x} + \int_{\partial\tau} \alpha(\mathbf{x}) \frac{\partial u_h}{\partial \mathbf{n}} \, ds = - \int_{\partial\tau} \alpha(\mathbf{x}) \frac{\partial(u - u_h)}{\partial \mathbf{n}} \, ds.$$

Since  $\mathcal{T}_h$  is a shape-regular partition, for all  $\tau \in \mathcal{T}$ , by the trace theorem and the Schwarz inequality,

$$\left\| \frac{\partial(u - u_h)}{\partial \mathbf{n}} \right\|_{L^2(\partial\tau)} \lesssim h_{\tau}^{-1/2} |u - u_h|_{H^1(\tau)} + h_{\tau}^{1/2} |u - u_h|_{H^2(\tau)},$$

where  $h_{\tau} = \text{diam}(\tau) \sim |\tau|^{1/d}$ . The fact that  $u \in H^{k+1}(\Omega)$  yields  $u - u_h \in H^{k+1}(\tau)$  for all  $\tau \in \mathcal{T}_h$ . By [1, Theorem 4.14], as  $\tau$  is shape-regular, we have

$$\begin{aligned} |u - u_h|_{H^2(\tau)} &\lesssim h_{\tau}^{-2+d/2} |\hat{u} - \hat{u}_h|_{H^2(\hat{\tau})} \\ &\lesssim h_{\tau}^{-2+d/2} \left( |\hat{u} - \hat{u}_h|_{H^1(\hat{\tau})} + |\hat{u} - \hat{u}_h|_{H^{k+1}(\hat{\tau})} \right) \\ &\lesssim h_{\tau}^{-1} |u - u_h|_{H^1(\tau)} + h_{\tau}^{k-1} |u - u_h|_{H^{k+1}(\tau)} \\ &= h_{\tau}^{-1} |u - u_h|_{H^1(\tau)} + h_{\tau}^{k-1} |u|_{H^{k+1}(\tau)}, \end{aligned}$$

where  $\hat{\tau}$  is the reference triangle or tetrahedron, see (3.9). Thus, it follows that

$$|u - u_h|_{H^2(\tau)} \lesssim h_{\tau}^{-1} |u - u_h|_{H^1(\tau)} + h_{\tau}^{k-1} |u|_{H^{k+1}(\tau)}.$$

Therefore, by (2.6),

$$(2.7) \quad \left| \int_{\tau} f \, d\mathbf{x} + \int_{\partial\tau} \alpha(\mathbf{x}) \frac{\partial u_h}{\partial \mathbf{n}} \, ds \right| \leq h_{\tau}^{1/2} \|\alpha(\mathbf{x})\|_{L^{\infty}(\Omega)} \left\| \frac{\partial(u - u_h)}{\partial \mathbf{n}} \right\|_{L^2(\partial\tau)} \\ \lesssim |u - u_h|_{H^1(\tau)} + h_{\tau}^k |u|_{H^{k+1}(\tau)}.$$

Summing up the above inequalities for all  $\tau \in \mathcal{T}$  and using the optimal order approximation property that

$$(2.8) \quad |u - u_h|_{H^1(\Omega)} \leq h^k |u|_{H^{k+1}(\Omega)},$$

the inequality (2.5) follows.  $\square$

**Remark 2.2.** *A similar estimate has been derived in [24] for  $P_1$  finite element solutions. In [24], on the dual-cell, one order higher convergence is proved for the local flux:*

$$\sum_{\mathbf{x}_i \in \text{vertex}(\mathcal{T}_h)} \left| \int_{S_{\mathbf{x}_i}} f \, d\mathbf{x} + \int_{\partial S_{\mathbf{x}_i}} \alpha(\mathbf{x}) \frac{\partial u_h}{\partial \mathbf{n}} \, ds \right| \lesssim h |u|_{H^2(\Omega)},$$

where  $S_{\mathbf{x}_i} = \cup_{\mathbf{x}_i \in \tau} \{\lambda_i \geq \lambda_j\}$ , see the left figure in Figure 1. Here  $\lambda_i$  is the barycentric-centric coordinate on  $\tau$  associated with vertex  $\mathbf{x}_i$ , cf. (3.1). This is because there is a supercloseness between the  $P_1$  finite element solution and the finite volume solution, and because the flux-error is identically 0 on each vertex-centered control volume  $S_{\mathbf{x}_i}$  for the finite volume solution. Here we give an unified estimate for element-wise fluxes of FEM solutions of any order.

As a direct consequence of (2.7) and (2.8), we have the following estimate for the  $L^2$  norm of numerical fluxes of FEM solutions.

**Corollary 2.3.** *Let  $u \in H^{k+1}(\Omega)$  solve (2.1)–(2.2) and  $u_h$  solve (2.4). It holds that*

$$\left( \sum_{\tau \in \mathcal{T}_h} \left| \int_{\tau} f \, d\mathbf{x} + \int_{\partial\tau} \alpha(\mathbf{x}) \frac{\partial u_h}{\partial \mathbf{n}} ds \right|^2 \right)^{1/2} \lesssim h^k |u|_{H^{k+1}(\Omega)}.$$

*Proof.* By (2.7),

$$\left| \int_{\tau} f \, d\mathbf{x} + \int_{\partial\tau} \alpha(\mathbf{x}) \frac{\partial u_h}{\partial \mathbf{n}} ds \right|^2 \lesssim |u - u_h|_{H^1(\tau)}^2 + h_{\tau}^k |u|_{H^{k+1}(\tau)}^2.$$

Combining them on all elements, we get

$$\begin{aligned} \left( \sum_{\tau \in \mathcal{T}_h} \left| \int_{\tau} f \, d\mathbf{x} + \int_{\partial\tau} \alpha(\mathbf{x}) \frac{\partial u_h}{\partial \mathbf{n}} ds \right|^2 \right)^{1/2} &\lesssim \left( |u - u_h|_{H^1(\Omega)}^2 + h^k |u|_{H^{k+1}(\Omega)}^2 \right)^{1/2} \\ &\lesssim |u - u_h|_{H^1(\Omega)} + h^k |u|_{H^{k+1}(\Omega)}. \end{aligned}$$

The corollary is proved by the optimal-order projection property (2.8) of the finite element solution.  $\square$

### 3. CONSTRUCTION OF FLUX-CONSERVING FINITE ELEMENT SOLUTIONS

In this section, we present an algorithm to process the FEM solution so that the flux is elementwise conserving.

Let the  $d$ -dimensional bubble function be

$$(3.1) \quad b_{\tau} = (d+1)^{d+1} \lambda_1 \dots \lambda_{d+1},$$

on a triangle or tetrahedron  $\tau \in \mathcal{T}$ . Here  $\{\lambda_i, i = 1, \dots, d+1\}$  are the barycentric coordinates on  $\tau$ . That is,  $\lambda_i(\mathbf{x})$  is a linear function defined by

$$\lambda_i(\mathbf{x}_j) = \delta_{ij} \quad \text{at } (d+1) \text{ vertices } \{\mathbf{x}_j\} \text{ of simplex } \tau.$$

By the divergence-theorem,

$$(3.2) \quad \int_{\tau} \Delta b_{\tau} \, d\mathbf{x} = \int_{\partial\tau} \frac{\partial b_{\tau}}{\partial \mathbf{n}} \, ds \gtrsim h^{d-2},$$

noting that  $\partial b_{\tau} / \partial \mathbf{n} > 0$  on  $\partial\tau$  except the  $(d+1)$  vertices. The scaling argument would give

$$(3.3) \quad \|b_{\tau}\|_{H^1(\tau)} \lesssim h^{-1} \|b_{\tau}\|_{L^2(\tau)} \lesssim h^{d-1}, \quad \text{in } d\text{-dimension.}$$

**Algorithm 3.1.** Given the problem (2.1)–(2.2) and a finite element space (2.3).

**Step 1.** Solve the finite element system

$$a(u_h, v_h) = (f, v_h), \quad \forall v_h \in U_h$$

to obtain the standard finite element solution  $u_h \in U_h$ .

**Step 2.** Correct  $u_h$  to obtain a flux-conserving solution:

$$(3.4) \quad \tilde{u}_h = u_h + \sum_{\tau \in \mathcal{T}_h} \gamma_\tau b_\tau,$$

where  $b_\tau$  is defined in (3.1) and

$$(3.5) \quad \gamma_\tau = \left( \int_{\partial\tau} \alpha(\mathbf{x}) \frac{\partial b_\tau}{\partial \mathbf{n}} ds \right)^{-1} \left( - \int_\tau f d\mathbf{x} - \int_{\partial\tau} \alpha(\mathbf{x}) \frac{\partial u_h}{\partial \mathbf{n}} ds \right) \quad \tau \in \mathcal{T}_h.$$

**Remark 3.2.** The post-processed solution  $\tilde{u}_h$  satisfies the local flux-conservation property,

$$\begin{aligned} \int_{\partial\tau} \alpha(\mathbf{x}) \frac{\partial(u - \tilde{u}_h)}{\partial \mathbf{n}} ds &= - \int_\tau f d\mathbf{x} - \int_{\partial\tau} \alpha(\mathbf{x}) \frac{\partial \tilde{u}_h}{\partial \mathbf{n}} ds \\ &= - \int_\tau f d\mathbf{x} - \int_{\partial\tau} \alpha(\mathbf{x}) \frac{\partial u_h}{\partial \mathbf{n}} ds - \gamma_\tau \int_{\partial\tau} \alpha(\mathbf{x}) \frac{\partial b_\tau}{\partial \mathbf{n}} ds \\ &= 0 \end{aligned}$$

for all  $\tau \in \mathcal{T}$ .

**Remark 3.3.** We use the lowest-order bubble functions in Algorithm 3.1, i.e., degree-3 bubbles in 2D and degree-4 in 3D. We can use nearly any bubble in the flux-correction, even non-polynomial bubbles. In the analysis below, we only require a bubble to be zero on the boundary and to have non-zero total flux on the boundary of an element, cf. (3.2). Although we use the lower order bubble, but it does not deteriorate the approximation of high order finite element. That is, for example, we can apply a degree-3 bubble correction to a 4-th degree finite element solution.

We next analyze the convergence property of the flux-conserving solution  $\tilde{u}_h$ .

**Theorem 3.4.** If  $u \in H^{k+1}(\Omega)$ , then the flux-conserving solution  $\tilde{u}_h$  defined in (3.4) approximates  $u$  in the optimal order,

$$(3.6) \quad |u - \tilde{u}_h|_{H^1(\Omega)} \lesssim h^k |u|_{H^{k+1}(\Omega)}$$

and

$$(3.7) \quad \|u - \tilde{u}_h\|_{L^2(\Omega)} \lesssim h^{k+1} |u|_{H^{k+1}(\Omega)}.$$

*Proof.* Since  $\alpha(\mathbf{x}) \geq \alpha_0 > 0$ , for all  $\tau \in \mathcal{T}$ ,

$$\int_{\partial\tau} \alpha(\mathbf{x}) \frac{\partial b_\tau}{\partial \mathbf{n}} ds \sim h^{d-2}.$$

By (3.5) and estimates in Theorem 2.1,

$$(3.8) \quad |\gamma_\tau| \lesssim h^{d-2} (|u - u_h|_{H^1(\tau)} + h^k |u|_{H^{k+1}(\tau)}).$$

On the other hand, since  $\tau \in \mathcal{T}_h$  is shape regular,

$$\|b_\tau\|_{L^2(\tau)} \sim |\tau|^{1/2} = h^{\frac{d}{2}}$$

and

$$|b_\tau|_{H^1(\tau)} \sim h_\tau^{-1} |\tau|^{1/2} \sim h_\tau^{\frac{d}{2}-1}.$$

Therefore, the correction part of  $\tilde{u}$  is bounded by

$$\begin{aligned} \left| \sum_{\tau \in \mathcal{T}} \gamma_\tau b_\tau \right|_{H^1(\Omega)}^2 &= \sum_{\tau \in \mathcal{T}_h} \gamma_\tau^2 |b_\tau|_{H^1(\tau)}^2 \\ &\lesssim \sum_{\tau \in \mathcal{T}} \gamma_\tau^2 h_\tau^{d-2} \sim h^{d-2} \sum_{\tau \in \mathcal{T}} \gamma_\tau^2. \end{aligned}$$

By (3.7) and (3.5),

$$\sum_{\tau \in \mathcal{T}} \gamma_\tau^2 \lesssim h^{2k} |u|_{H^{k+1}(\Omega)}^2.$$

Similarly, by the scaling argument,

$$\left\| \sum_{\tau \in \mathcal{T}_h} \gamma_\tau b_\tau \right\|_{L^2(\Omega)}^2 \lesssim h^{2k+2} |u|_{H^{k+1}(\Omega)}^2.$$

By the triangle inequalities

$$\begin{aligned} |u - \tilde{u}_h|_{H^1(\Omega)} &\leq |u - u_h|_{H^1(\Omega)} + \left| \sum_{\tau \in \mathcal{T}} \gamma_\tau b_\tau \right|_{H^1(\Omega)}, \\ \|u - \tilde{u}_h\|_{L^2(\Omega)} &\leq \|u - u_h\|_{L^2(\Omega)} + \left\| \sum_{\tau \in \mathcal{T}} \gamma_\tau b_\tau \right\|_{L^2(\Omega)}, \end{aligned}$$

and the standard finite elements estimates on  $u_h$  (cf. [3]), the estimates (3.6) and (3.7) follow.  $\square$

The corrected solution  $\tilde{u}_h$ , defined by (3.4), does not satisfy the original finite element equations (2.4) any more, though it remains as an optimal-order solution. We can improve the method by using high-order, orthogonal bubble functions. Let

$$(3.9) \quad \hat{\tau} = \{(x, y) \mid x, y, 1 - x - y \geq 0\}$$

be the reference triangle, i.e., the unit right triangle at the origin. Let  $\hat{b}^{(k)} \in \mathcal{P}_k(\hat{\tau})$  such that

$$\begin{aligned} \hat{b}^{(k)}(\mathbf{x}) &= 0 \quad \text{on } \partial\hat{\tau}, \\ \int_{\hat{\tau}} \hat{b}^{(k)} \Delta p_{k-2} d\mathbf{x} &= 0 \quad \forall p_{k-2} \in \mathcal{P}_{k-2}(\hat{\tau}), \\ \int_{\hat{\tau}} \Delta \hat{b}^{(k)} d\mathbf{x} &\neq 0. \end{aligned}$$

We note that, by writing  $\hat{b}^{(k)} = b_{\hat{\tau}} \hat{p}_{k-3}$ , there are  $\dim \mathcal{P}_{k-3} = (k-1)(k-2)/2$  degrees of freedom in constructing  $\hat{b}^{(k)}$  but only  $\dim(\Delta \mathcal{P}_{k-2}) + 1 = (k-2)(k-3)/2 + 1$

constraints in the constructions. For example, we can let

$$(3.10) \quad \hat{b}^{(k)}(\mathbf{x}) = \begin{cases} b_{\hat{\tau}}, & k = 3, \\ (3x + 3y - 2)b_{\hat{\tau}}, & k = 4, \\ (x^2 - 3xy + y^2)b_{\hat{\tau}}, & k = 5, \\ (2x^2 - 6xy + 2y^2 \\ + x^3 - 16x^2y + 26xy^2 - 6y^3)b_{\hat{\tau}}, & k = 6, \\ (x^4 - 10x^3y + 20x^2y^2 - 10xy^3 + y^4)b_{\hat{\tau}}, & k = 7, \\ (3x^4 - 30x^3y + 60x^2y^2 - 30xy^3 + 3y^4 \\ + 3x^5 - 66x^4y + 290x^3y^2 \\ - 360x^2y^3 + 129xy^4 - 10y^5)b_{\hat{\tau}}, & k = 8, \end{cases}$$

where  $b_{\hat{\tau}}$  is defined in (3.1). By the construction, the bubble functions are orthogonal to the finite element functions in  $U_h$ , in semi- $H^1$  inner-product:

$$\begin{aligned} \int_{\tau} \nabla b_{\tau} \nabla v_h \, d\mathbf{x} &= \int_{\hat{\tau}} \hat{\nabla}^T \hat{b}^{(k+2)} (JF)^{-T} (JF)^{-1} \hat{\nabla} \hat{v}_h |J| \, d\hat{\mathbf{x}} \\ &= - \int_{\hat{\tau}} \hat{b}^{(k+2)} \hat{\nabla} \cdot ((JF)^{-T} (JF)^{-1} \hat{\nabla} \hat{v}_h |J|) \, d\hat{\mathbf{x}} \\ &= - \int_{\hat{\tau}} \hat{b}^{(k+2)} p_{k-2} \, d\hat{\mathbf{x}} = 0, \end{aligned}$$

where  $v_h \in U_h$  is a degree- $k$  polynomial on  $\tau$  and  $p_{k-2}$  is another degree- $(k-2)$  polynomial on  $\hat{\tau}$ . Thus, if  $b_{\tau}$  in (3.4) is replaced by the above orthogonal-bubbles (3.10), then the processed finite element solution still satisfies the original equations (2.4):

$$a(\tilde{u}_h, v_h) = (\nabla u_h, \nabla v_h) + \sum_{\tau \in \mathcal{T}_h} \gamma_{\tau} (\nabla b_{\tau}^{(k+2)}, \nabla v_h) = (\nabla u_h, \nabla v_h) = (f, v_h)$$

for all  $v_h \in U_h$ . Here we assumed a constant coefficient  $\alpha(\mathbf{x}) \equiv \alpha_0$ . For variable coefficient  $\alpha(\mathbf{x})$ , the orthogonal bubbles can be constructed element by element.

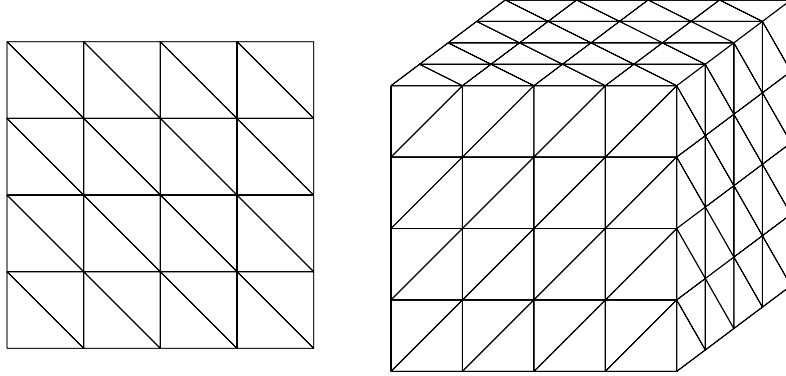


FIGURE 2. The grid 3 in 2D and 3D  $h = 1/4$ , cf. Tables 1–5.



## 4. NUMERICAL EXPERIMENTS

We provide two numerical tests. The exact solutions, in 2D and 3D, are

$$(4.1) \quad u(x, y) = 2^8 x^2 (1-x)^2 y^2 (1-y)^2,$$

$$(4.2) \quad u(x, y) = 2^6 x(1-x)y(1-y)z(1-z),$$

respectively. We solve the Poisson equation, i.e., (2.1) with  $\alpha(\mathbf{x}) \equiv 1$  on the domain,  $(0, 1)^2$  and  $(0, 1)^3$ . The third level grids in 2D and 3D computation are shown in Figure 2. Here we use (multigrid) nested refinement to generate grids, cf. [25]. We choose a high order polynomial as an exact solution in 2D (4.1) only to avoid exact finite element solutions when using higher degree elements.

TABLE 1. The order of convergence for the  $P_1$  element.

	$ e_h _{H^1}$	$h^n$	$ E_h _*$	$h^n$	$ \tilde{e}_h _{H^1}$	$h^n$	$ \tilde{E}_h _*$	$h^n$	#cg	dof
2	0.08333	0.0	5.000	0.0	0.387	0.7	0.00000000	0.7	2	9
3	0.11282	0.0	5.102	0.0	0.209	0.9	0.00000000	0.7	6	25
4	0.03590	1.7	5.186	0.0	0.107	1.0	0.00000000	0.0	26	81
5	0.00953	1.9	5.207	0.0	0.053	1.0	0.00000000	0.4	55	289
6	0.00242	2.0	5.211	0.0	0.026	1.0	0.00000000	0.1	111	1089

In the data tables, we use the following notations:

$$e_h = I_h u - u_h,$$

$$E_h = u - u_h,$$

$$\tilde{e}_h = I_h u - \tilde{u}_h,$$

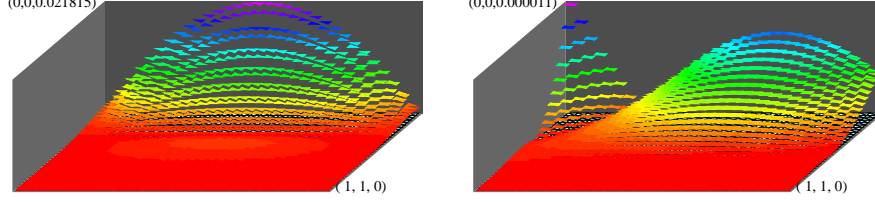
$$\tilde{E}_h = u - \tilde{u}_h,$$

where  $I_h$  is the nodal value interpolation operator,  $u_h$  is the finite element solution defined in (2.4), and  $\tilde{u}_h$  is the post-processed finite element solution defined in (3.4). Also we use the following norm to measure the error in the total flux:

$$(4.3) \quad |E_h|_* = \sum_{\tau \in \mathcal{T}_h} \left| \int_{\partial\tau} \frac{\partial(u - u_h)}{\partial \mathbf{n}} ds \right| = \sum_{\tau \in \mathcal{T}_h} \left| \int_{\tau} f d\mathbf{x} + \int_{\partial\tau} \frac{\partial u_h}{\partial \mathbf{n}} ds \right|.$$

In all our computation, we use the conjugate gradient method to solve the linear systems of finite element equations. As the grids are not very fine, the conjugate gradient method is comparable to the optimal order solve, the multigrid method. Thus, we list the number of conjugate gradient iterations by #cg in the data tables.

In Table 1, we can see from the 4th column that there is no flux convergence for the linear finite element in 2D, confirming Theorem 2.1. However, the total flux error defined in (4.3) is completely zero, other than quadrature formula differences, by the 8th column data in Table 1. We note that even though there is no convergence for  $P_1$  finite element in total flux, but pointwise flux-error of  $P_1$  finite

FIGURE 3. The flux-error (4.3) for  $P_1$  and for  $P_3$  FEM, for (4.1).

element solution does converge to zero when  $h$  goes to 0. It depends on the way we measure the error. Since the total inter-element boundary grows at rate  $h^{-1}$  in 2D, the pointwise flux-error has to converge at a rate higher than  $h^1$ . To show this, we plot the flux-error (4.3) elementwise as a constant in Figure 3. Where on the left, we used  $P_1$  FEM, and  $P_3$  FEM on the right. The  $L^\infty$  flux-error is  $O(h)$  for  $P_1$  FEM, and  $O(h^4)$  for  $P_3$  FEM. This is not proved in this paper.

We note that there is a superconvergence in semi- $H^1$  norm for  $P_1$  finite element, shown in second column of Table 1. But after flux-correction, such a superconvergence no longer holds (6-th column).

TABLE 2. The errors for the  $P_4$  element in 2D.

	$ e_h _{H^1}$	$h^n$	$ E_h _*$	$h^n$	$ \tilde{e}_h _{H^1}$	$h^n$	$ \tilde{e}_h^{(6)} _{H^1}$	$h^n$
1	0.1291516	0.0	1.19696	0.0	0.1837393	0.0	17.35203	0.0
2	0.0274134	2.2	0.30318	2.0	0.0261514	2.8	2.26847	2.9
3	0.0025223	3.4	0.04526	2.7	0.0021648	3.6	0.17589	3.7
4	0.0001742	3.9	0.00584	3.0	0.0001448	3.9	0.01054	4.1
5	0.0000112	4.0	0.00073	3.0	0.0000092	4.0	0.00059	4.1
6	0.0000007	4.0	0.00009	3.0	0.0000005	4.0	0.00003	4.1

Next, we use the 2D  $P_4$  finite element. The data are listed in Table 2. This time, the finite element solution does not have a superconvergence. So the order of error before and after flux-correction are the same, order 4, the optimal order. However, the finite element does converge in approximating the total flux, but of order 3, shown in the 6th column of Table 2, conforming Theorem 2.1 again. We repeat the computation for  $P_4$  FEM but with orthogonal bubbles  $\hat{\tau}^{(6)}$  defined in (3.10). This time,  $\tilde{u}_h$  remains as a solution to the original finite element equations (2.4). The convergence is shown in the eighth column of Table 2. Again, both the processed finite element solutions have a zero error in total flux and both keep the optimal order of FEM approximation.

Next, we do a 3D computation. As in 2D, when using linear finite element, there is no convergence in total-flux approximation, shown in the 6th column of

TABLE 3. The order of convergence for the  $P_1$  element in 3D.

	$\ e_h\ _{L^2}$	$h^n$	$ e_h _{H^1}$	$h^n$	$ E_h _*$	$h^n$	#cg
2	0.11180	0.0	0.86603	0.0	10.66667	0.0	2
3	0.06044	0.9	0.37530	1.2	10.66667	0.0	5
4	0.01871	1.7	0.10743	1.8	10.66667	0.0	24
5	0.00494	1.9	0.02780	2.0	10.66667	0.0	49
6	0.00125	2.0	0.00701	2.0	10.66667	0.0	93
	$\ \tilde{e}_h\ _{L^2}$	$h^n$	$ \tilde{e}_h _{H^1}$	$h^n$	$ \tilde{E}_h _*$	$h^n$	dof
1	0.05514	0.0	61.58403	0.0	0.00000	0.0	8
2	0.10502	0.0	16.41392	1.9	0.00000	0.0	27
3	0.05780	0.9	4.29661	1.9	0.00000	0.0	125
4	0.01800	1.7	1.08916	2.0	0.00000	0.0	729
5	0.00477	1.9	0.27328	2.0	0.00000	0.0	4913
6	0.00121	2.0	0.06838	2.0	0.00000	0.0	35937

Table 3. As shown by Theorem 3.4, the post-processed finite element solution converges with the optimal order in  $L^2$  and  $H^1$  norm, shown in the second half of Table 3. Due to a large flux-error, the correction bubbles cause a much bigger error in energy norm, i.e., semi- $H^1$  norm, see 4th column in Tables 3–5. More comments are made below. However, the correction does not change the FEM solution on all inter-element triangles, i.e.,  $u_h = \tilde{u}_h$  there. Note that the error of corrected solution in energy norm is comparable to that of the original finite element solution, or even smaller, in 2D, see Tables 1–2.

TABLE 4. The order of convergence for the  $P_3$  element in 3D.

	$\ e_h\ _{L^2}$	$h^n$	$ e_h _{H^1}$	$h^n$	$ E_h _*$	$h^n$	#cg
1	0.06162	0.0	0.37386	0.0	2.50980	0.0	3
2	0.00610	3.3	0.08622	2.1	0.94217	1.4	20
3	0.00037	4.1	0.01297	2.7	0.21351	2.1	54
4	0.00002	4.1	0.00175	2.9	0.05201	2.0	98
5	0.00000	4.0	0.00023	3.0	0.01305	2.0	174
	$\ \tilde{e}_h\ _{L^2}$	$h^n$	$ \tilde{e}_h _{H^1}$	$h^n$	$ \tilde{E}_h _*$	$h^n$	dof
1	0.05273	0.0	14.49518	0.0	0.00000	0.0	64
2	0.00656	3.0	1.53168	3.2	0.00000	0.0	343
3	0.00040	4.0	0.09738	4.0	0.00000	0.0	2197
4	0.00002	4.0	0.00631	3.9	0.00000	0.0	15625
5	0.00000	4.0	0.00044	3.8	0.00000	0.0	117649

Now, if we use degree 3 finite element in 3D, we would have order 2 convergence for the total flux, shown in Table 4. We note that the flux-corrected finite element

solution also converges at order 3 in semi- $H^1$  norm. But it looks like, in Table 4, that the order of the flux-corrected finite element solution is higher than 3. It is caused by higher order error in flux. It seems the bubble term  $u_b$  (see (4.4)) converges to 0 at a higher order in this case. Comparing the errors in column 4 in top and bottom table of Table 4, we would predict the order of  $|\tilde{e}_h|_{H^1}$  would return to 3 once it catches  $|e_h|_{H^1}$ . This can be seen in Table 5. When using the 5th degree finite element, the bubble functions are inside the finite element space. Then it is known from the finite element projection property that

$$(4.4) \quad |E_h|_{H^1} \leq |\tilde{E}_h|_{H^1} \leq |E_h|_{H^1} + |u_b|_{H^1},$$

where  $u_b = \sum_{\tau \in \mathcal{T}} \gamma_\tau b_\tau$  is the bubble correction term. Thus, the order of converges of  $|\tilde{E}_h|_{H^1}$  would return to that of  $|E_h|_{H^1}$  when the correction  $|u_b|_{H^1}$  is no longer dominant, see column 4 in the second half of Table 5.

TABLE 5. The order of convergence for the  $P_5$  element in 3D.

	$\ e_h\ _{L^2}$	$h^n$	$ e_h _{H^1}$	$h^n$	$ E_h _*$	$h^n$	#cg
1	0.00927	0.0	0.11994	0.0	0.12616	0.0	12
2	0.00014	6.1	0.00382	5.0	0.00815	4.0	77
3	0.00000	6.1	0.00012	5.0	0.00052	4.0	159
4	0.00000	6.0	0.00000	5.0	0.00003	4.0	290
5	0.00000	6.0	0.00000	5.0	0.00000	4.0	505
	$\ \tilde{e}_h\ _{L^2}$	$h^n$	$ \tilde{e}_h _{H^1}$	$h^n$	$ \tilde{E}_h _*$	$h^n$	dof
1	0.00927	0.0	0.73820	0.0	0.00000	0.0	216
2	0.00014	6.1	0.01242	5.9	0.00000	0.0	1331
3	0.00000	6.1	0.00022	5.8	0.00000	0.0	9261
4	0.00000	6.0	0.00000	5.5	0.00000	0.0	68921
5	0.00000	6.0	0.00000	5.2	0.00000	0.0	531441

## 5. CONCLUDING REMARKS

The main motivation in designing FVM is the flux-conservation, a desirable property in many scientific disciplines such as CFD. However, on one side, the accuracy analysis for high order FVM schemes is hard to be established. On the other hand, the linear algebraic system resulting from the FVM scheme is often non-symmetric, even if the PDE to be solved is self-adjoint.

In this paper, we propose post-processing techniques for FEM solutions. The new solution preserves both local conservation laws and overall accuracy. Besides, comparing to the complex construction of FVM schemes and high-cost computation of non-symmetric linear systems, any existing finite element code can use our method by adding a simple subroutine to perform the post-processing. In this

sense, the techniques presented in this paper provide a better option, at least for elliptic problems.

Of course we do not mean that we should abandon the FVM for elliptic equations. In a recent study of high-order FVM schemes for 1D elliptic equations [4], it is found that the derivative of the FVM solutions has higher order superconvergence property than that of the corresponding FEM solutions at some so-called “optimal stress points”. On the other side, our post processing techniques may even deteriorate the superconvergence property of the original FEM solution. In other words, the FVM schemes may still have their advantages for elliptic equations.

#### REFERENCES

- [1] Adams, R. A. Sobolev spaces. Pure and Applied Mathematics, Vol. 65. Academic Press, New York-London, 1975.
- [2] Bank, R. E.; Rose, D. J. Some error estimates for the box method. *SIAM J. Numer. Anal.* 24 (1987), 777–787.
- [3] Brenner, S. C.; Scott, L. R. The mathematical theory of finite element methods. Third edition. Texts in Applied Mathematics, 15. Springer, New York, 2008.
- [4] Cao, W.; Zhang, Z.; Zou, Q. Superconvergence finite volume schemes for 1D elliptic equations. 2011, preprint.
- [5] Cai, Z. On the finite volume element method. *Numer. Math.* 58 (1991), no. 7, 713–735.
- [6] Cai, Z.; Douglas, J., Jr.; Park, M. Development and analysis of higher order finite volume methods over rectangles for elliptic equations. Challenges in computational mathematics (Pohang, 2001). *Adv. Comput. Math.* 19 (2003), no. 1-3, 3–33.
- [7] Cai, Z.; Mandel, J.; McCormick, S. The finite volume element method for diffusion equations on general triangulations. *SIAM J. Numer. Anal.* 28 (1991), no. 2, 392–402.
- [8] Chen, L. A new class of high order finite volume methods for second order elliptic equations. *SIAM J. Numer. Anal.* 47 (2010), no. 6, 4021–4043.
- [9] Chen, Z.; Wu, J.; Xu, Y. Higher-order finite volume methods for elliptic boundary value problems. *Adv. in Comput. Math.*, in Press.
- [10] Dai, X.; Gong, X.; Yang, Z.; Zhang, D.; Zhou, A. Finite volume discretizations for eigenvalue problems with applications to electronic structure calculations. *Multiscale Model. Simul.* 9 (2011), no. 1, 208–240.
- [11] Ewing, R. E.; Lin, T.; Lin, Y. On the accuracy of finite volume element method based on piecewise linear polynomials. *SIAM J. Numer. Anal.* 39 (2002), 1865–1888.
- [12] Eymard, R.; Gallouet, T.; Herbin, R. Finite Volume Methods, vol. 7. North Holland, Amsterdam, 2000.
- [13] Hackbusch, W. On first and second order box methods. *Computing* 41 (1989), 277–296.
- [14] Hermeline, F. A finite volume method for approximating 3D diffusion operators on general meshes. *J. Comput. Phys.* 228 (2009), no. 16, 5763–5786.
- [15] LeVeque, R. J. Finite volume methods for hyperbolic problems. Cambridge Texts in Applied Mathematics. Cambridge University Press, Cambridge, 2002.
- [16] Li, R.; Chen, Z.; Wu, W. The Generalized Difference Methods for Partial Differential Equations (Numerical Analysis of Finite Volume Methods). Marcel Dekker, New York, 2000.
- [17] Li, Y.; Shu, S.; Xu, Y.; Zou, Q. Multilevel preconditioning for the finite volume method. *Math. Comp.*, in press.
- [18] Liebau, F. The finite volume element method with quadratic basis functions. *Computing* 57 (1996), no. 4, 281–299.
- [19] Noelle, S.; Xing, Y.; Shu, C.-W. High-order well-balanced finite volume WENO schemes for shallow water equation with moving water. *J. Comput. Phys.* 226 (2007), no. 1, 29–58.
- [20] Plexousakis, M.; Zouraris, G. On the construction and analysis of high order locally conservative finite volume type methods for one dimensional elliptic problems, *SIAM J. Numer. Anal.* 42 (2004), 1226–1260.
- [21] Scott, L. R.; Zhang, S. Higher-dimensional nonnested multigrid methods. *Math. Comp.* 58 (1992), no. 198, 457–466.

- [22] Tian, M.; Chen, Z. Quadratical element generalized differential methods for elliptic equations. *Numer. Math. J. Chinese Univ.* 13 (1991), 99–113.
- [23] Vogel, A.; Xu, J.; Wittum, G. A generalization of the vertex-centered finite volume scheme to arbitrary high order. *Comput. Vis. Sci.* 13 (2010), no. 5, 221–228.
- [24] Xu, J.; Zou, Q. Analysis of linear and quadratic simplicial finite volume methods for elliptic equations. *Numer. Math.*, 111 (2009), 469–492.
- [25] Zhang, S. Successive subdivisions of tetrahedra and multigrid methods on tetrahedral meshes. *Houston J. of Math.* 21 (1995), 541–556.

DEPARTMENT OF MATHEMATICAL SCIENCES, UNIVERSITY OF DELAWARE, NEWARK, DE 19716, USA. SZHANG@UDEL.EDU

DEPARTMENT OF MATHEMATICS, WAYNE STATE UNIVERSITY, DETROIT, MI 48202, USA. AG7791@WAYNE.EDU

DEPARTMENT OF SCIENTIFIC COMPUTATION AND COMPUTERS' APPLICATIONS AND GUANG-DONG PROVINCE KEY LABORATORY OF COMPUTATIONAL SCIENCE, SUN YAT-SEN UNIVERSITY, GUANGZHOU, 510275, CHINA. MCSZQS@MAIL.SYSU.EDU.CN